ORIGINAL PAPER

Fabrication of electrospun polyamide–weathered basalt nano-composite as a non-conventional membrane for basic and acid dye removal

M. N. El-Sheikh[1] · Bahaa S. Metwally[2] · Mahmoud. F. Mubarak[3] · Hanan A. Ahmed[4] · Thanaa Abdel Moghny[3] · Ahmed M. Zayed[5]

Abstract

In this study, an adsorptive electrospun polyamide membrane (ESPA) and electrospun polyamide–weathered basalt composite membrane (ESPA-WB) were prepared by an electrospinning process at room temperature. Hence, the WB structure was built as a polymeric membrane separation film in combination with the ESPA matrix as a composite nano-filtration membrane. Then, the ESPA and ESPA-WB membranes were characterized using BET surface area analysis, Fourier transform infrared spectroscopy, X-ray diffraction, and scanning electron microscopy (SEM). To avoid cracks forming during the sintering process, the WB should be added in certain percentages. The microstructures of the prepared membranes were investigated to evaluate their efficiency for basic and acidic dyes' removal and their permeation flux. Compared with the ESPA, the ESPA-WB membrane combines the characteristics of WB and ESPA, which greatly enhances the performance of both methylene blue (MB) and methyl orange (MO) dyes removal from synthetic wastewater. The outcomes of this study indicated that the dye uptake in the case of ESPA-WB is

✉ Mahmoud. F. Mubarak
  fathy8753@yahoo.com; fathy9853@epri.sci.eg

✉ Ahmed M. Zayed
  zayed_2000eg@yahoo.com; ahmed.zayed@science.bsu.edu.eg

[1] Mechanical Department, Faculty of Technology and Education, Beni-Suef University, Beni-Suef, Egypt

[2] Textile Technology Department, Faculty of Technology and Education, Beni-Suef University, Beni-Suef, Egypt

[3] Petroleum Applications Department, Egyptian Petroleum Research Institute (EPRI), Ahmed El-Zomer, Nasr City, Cairo, Egypt

[4] Petrochemicals Department, Egyptian Petroleum Research Institute (EPRI), Ahmed El-Zomer, Nasr City, Cairo, Egypt

[5] Applied Mineralogy and Water Research Lab, Department of Geology, Faculty of Science, Beni-Suef University, Beni-Suef, Egypt

higher than that of ESPA, and it decreases with an increase in dye concentrations. The obtained membrane ESPA-WB showed both an excellent anti-dye fouling and a good rejection property for both dyes (i.e. 90% rejection for MB and 74% for MO) with no sign of contamination by the applied dyes. It was found that the structure of the ESPA-WB membrane contains a large number of several adsorption sites which leads to an increase in the removal rate of dyes. Hence, this study demonstrated a non-conventional strategy to prepare an effective adsorptive nano-composite membrane that can be applied as a highly recyclable one for the removal of organic dyes.

Graphic abstract
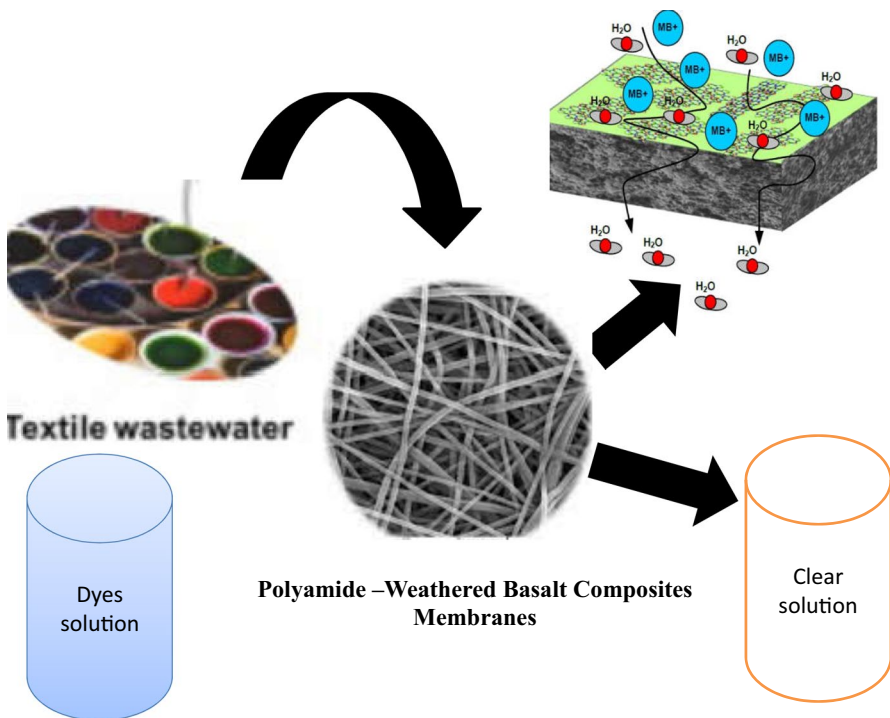
Keywords Electrospinning · Membrane · Dye · Filtration · Nano-composite

Introduction

Dyes are an important component in various industries such as food, pharmaceuticals, cosmetics, paper, plastics, leather, and textile finishing [1]. Textile dyeing is among the most environmentally unfriendly industries owing to the large quantities of water demanded and the strongly colored wastewater produced, polluted with dyes and other chemical auxiliaries [2].

Methyl orange (MO) anionic dye as a model compound for ordinary water-soluble azo-dyes which is widely utilized in most of the mentioned industries, is toxic and carcinogenic to animals and humans [3–5]. Also, azo-dyes are very stable due to greater bond strength, which prevents their degradation by the conventional treatment methods [6, 7].

Methylene blue (MB) cationic dye is a typical thiazine dye pollutant with the formula of ($C_{16}H_{10}N_3ClS$). It's widely utilized in many cellulose and protein textiles dyeing and causes harmful effects on aquatic organisms and humans [8]. The release of such highly colored dye effluents into the environment could pose a huge environmental risk to the water ecosystem and underground aquifers and thus to human health [4, 9]. Therefore, it is an essential requirement for the sustainability of the environmental ecosystem to remove azo-dyes and color from the aquatic systems using an environmentally friendly advanced technology. Although there are many purification technologies like adsorption [10], catalytic ozonation [11], biodegradation [12], photolysis [13] and electrochemical oxidation [14] applied to address this issue, achieving a higher treatment efficiency for the removal of dyes from colored wastewater is still a major concern [11]. The membrane separation process could be an eco-friendly alternative for treating the above-mentioned dyes; MO and MB as it can perform effective, selective, and reliable removal to protect water resources [4, 15].

Recently, nanofiber filtration membranes (NFM) revealed a higher rejection rate improving the filtration efficiency for small organic dye molecules. This was ascribed to their fascinating physicochemical and mechanical properties (e.g. high surface area, porosity, permeability, and good strengths) [16–19], as well as, the applicability to produce composites with other materials [20]. There are many methods to produce NFM such as blow spinning, centrifugal spinning, draw spinning, and electrospinning [21–24]. Among these methods, electrospinning is the most advanced technique for NFM fabrication due to its simplicity, low cost, a large selection of materials, strong versatility, and ability to produce nanofibers with small pore diameters [21, 25]. Electrospinning is a versatile technology that has been applied for the creation of ultrafine nonwoven fibrous membranes of a variety of materials, such as inorganic materials [26, 27], polymers [28, 29], and hybrid materials [30, 31]. These fibers exhibit diameters ranging from nanometers to micrometers with large ratios of surface area to volume and various hierarchical structures [32]. Electrospun nano-fiber membranes (ESNFMs) have high porosity, high specific surface area, and unique interconnected structure [33]. It has huge advantages and potential in the treatment and recycling of wastewater. Electrospun nano-fibers have seen a wide range of applications including filtration, catalysis, sensor, electronic and optical device, energy conversion and storage, and biomedical uses [33]. There are various polymers originating from synthetic and natural sources that have been processed into electrospun nano-fibers with various morphologies like silk fibroin [34], cellulose acetate (CA) [35], polycaprolactone [36], polystyrene [37], collagen [38], poly(methyl methacrylate) [39], poly(L-lactic acid) [40] and poly(vinyl alcohol) (PVA) [41]. Such fabricated nano-fibers can be used in air/ wastewater filtration. Also, Ding et al. [42] reported the application of the electrospinning method for the fabrication of functional electrospun nanofibers from variable polymers such

as polysulfone, polyvinylidene fluoride, and polyvinyl alcohol. The basic electrospinning setup consists of a spinneret with a metallic needle, a high-voltage power supply, and grounded collector. Polymer solution (or melt) is filled inside a plastic syringe, which is loaded into a syringe pump to form a droplet at the tip, the power supply is electrically charging the droplet, which is stretched many times and dries or solidifies to leave a polymeric nanofiber on grounded collector [43, 44]. With the utilization of the electrospinning process, the morphology of nanofibers can be easily adjusted by changing the number of variables. These variables can be separated into three main groups; solution parameters (polymer concentration, molecular weight, and conductivity) [44, 45], processing parameters (Applied voltage, flow rate, and tip to collector distance needle diameter) [46] at ambient conditions (atmospheric pressure and room temperature) [47].

On the other hand, due to the fast fashion cycle, enormous amounts of non-biodegradable synthetic textile wastes are annually produced from carpet factories causing serious environmental problems [48–50]. Among these textile wastes, polyamides (PA) are the most widely used in carpet factories, especially, PA6 and PA6.6 fibers that are used as face carpet yarns [51]. Polyamides (PAs) are versatile semi-crystalline polymers with high chemical resistance and good thermal and mechanical properties [52]. They are produced usually in the form of fibers, for use in a broad scope of applications (fashion, automotive, construction, packaging, electrical, electronic, and coatings industries) [53]. Therefore, polyamides represent an important proportion of polymer waste. As with the physical method, electrospinning offers the opportunity to prepare fibrous polymer products from post-industrial polymers. For example, poly (ethylene terephthalate)-based waste drinking bottles were used to fabricate electrospun fibers with an average diameter of 95–37 nm for filtration applications [54], while Isik et al. [55] obtained expanded polystyrene (EPS) from insulation and packing material without further purification.

Utilizing polyamide (PA) as base layers, various composite fibrous membranes were fabricated using different materials (e.g. zeolite, fresh basalt, carbon nanotubes, graphene oxide … etc. [56, 57]. Unlike the previously applied fresh basalt (FB) composed mainly of pyroxene, olivine, and calcic plagioclase as primary components with some subordinate magnetite, ilmenite, and nepheline minerals, the weathering processes to which the FB was subjected contributed to a noticeable appearance of clay minerals (e.g. montmorillonite, illite, and vermiculite) among its dominant components on the expense of the primary ones [58]. Consequently, such weathering products (WB) accumulate in huge reserves at the fresh basalt quarries in several localities in Egypt with no proper industrial application causing a cute environmental problem. These products are clay-like materials enriched in ferromagnesian metal oxide components.

So, to maximize the market value and mitigate the environmental problems generated by such industrial (PA 6.6) and natural (WB) wastes, these wastes were utilized in the fabrication of valuable electrospun nano-composite membranes (ESPA-WB). This nano-composite was applied in the removal process of both cationic and anionic dyes (MB and MO, orderly) from synthetic wastewater. As well, the removal mechanisms of these dyes by the current fabricated membrane (ESPA-WB) were carefully investigated and the role of the incorporated WB in the adsorption

process was highlighted. Similarly, the impact of different experimental parameters such as initial dye concentration, pH, pressure, and the involved electrolytes on the dye removal efficiency by the addressed nano-membrane was studied. Also, the life operation performance of this nano-filter membrane was evaluated.

Materials and experiments

Materials

Weathered basalt (WB) was obtained from the Western Desert (Egypt). Polyamide (PA6.6) waste was collected from an Egyptian carpet factory. Formic acid 90% was supplied from (BDH Chemicals, England). Methyl orange (MO) and methylene blue (MB) dyes were purchased from (Fluka, Switzerland). All dye stock solutions were prepared using deionized (DI) water. Most of the chemicals used in this research including NaOH, $CaCl_2$, $NaNO_3$, H_2SO_4 (98.0%), and HCl (32.0%) were purchased from Sigma-Aldrich Company.

Preparation of raw materials (WB and PA waste)

The collected WB samples were crushed by a ball mill machine (Retsch Pm 100, Germany) < 65 nm, then washed with deionized water (DI) to neutral pH, and finally dried in an oven at 70 °C for 24 h. The PA-fibers were washed with a non-ionic detergent solution (1 g/L) at 80 °C for 20 min, rinsed in DI to remove any impurities, and then air-dried at room temperature [59].

Fabrication of electrospun polyamide membrane (ESPA)

The electrospun polyamide membrane (ESPA) was fabricated using an electrospinning device that consists of a programmable mono-channel syringe pump (NE-4000, USA) and a high-voltage power supply (HVA b2 Electronics). In this regard, the waste polyamide fiber was dissolved in 90% formic acid at a concentration of 15 wt.% and stirred for 30 min at room temperature. Then the polyamide solution was fed to the 10 mL plastic syringe with a positively charged metallic micro-tip. The spinning process was conducted at a constant electric field (18 kV), fixed collecting distance, and flow rate (15 cm and 1.2 ml/h, orderly). The electrospun polyamide (ESPA) was collected on a negatively charged fixed collector. To maintain the thickness of the produced ESPA fixed (120–130 μm), the electro-spinning processes were performed for about 6 h at ambient temperature.

Fabrication of electrospun polyamide–weathered basalt nano-composite membrane (ESPA-WB)

To fabricate the desired ESPA-WB membrane the above mention protocol was applied with only one exception that include the addition of WB (< 63 nm) to be

completely dispersed in the dissolving reagent (formic acid) before the addition of PA to the mixture achieving a mass ratio of 1:4 (WB:PA) with continuous stirring for 30 processes at each addition.

For the above fabricated (ESPA), the WB was added to the spinning solution at a mass ratio of 1:4 (WB:PA) and stirred for 30 min.

Both fabricated membranes (ESPA and ESPA-WB) were rinsed with deionized water (DI) for 20 min then washed with a mixture of alcohol:water (30:70) to be neutralized before open air drying and packing for further application.

Preparation of stock solutions

One gram of each dye (MB and MO) was dissolved in 1000 mL of DI to prepare stock solutions with a concentration of 1000 ppm/L. The stock solutions were diluted separately using DI to prepare the required initial concentrations of both dyes (15–120 ppm).

Studies of the dye rejection with the variation of membrane parameters

Membrane performance and ultrafiltration setup

A High productivity filtration system (Millipore, model 8050) containing a filtration cell fitted with a membrane of a 3.14 cm^2 area was used to analyze the performance of prepared membranes. The system was pressurized with nitrogen (5–22 bar) and the feed solution was stirred continuously at 400 rpm to minimize concentration polarization. The stirred cell and reservoir of a total volume of 2 L were filled with dye solution at a variable pressure (5–22 bar) at an initial concentration of 120 ppm and pH value of 7 for dyes' solutions. The ultrafiltration setup is shown in Fig. 1. The pH feed dye solution was adjusted at the desired value by adding hydrochloric acid or sodium hydroxide solution (0.1 M) and kept in the range of 3–10. Also, the feed solution was adjusted at fixed pressure and initial concentration of 15 bar and 120 ppm, respectively. The dye concentration was varied (20, 30, 60, 120 ppm) at a feed pressure of 15 bar at a neutral pH value. Then, 15 mL of permeate solution was used to measure the remaining dye concentration using UV–Vis spectroscopy (UV-2500 PC, Shimazu). The effect of each ionic electrolyte concentration of NaCl, CaCl$_2$, and NaOH on both dyes was adjusted to 120 mg /L at a pressure of 15 bar and pH 6 and 8 for MB and MO, respectively. The electrolyte feed solution was measured using an ion chromatography technique (Metrohm 883 Basic. C.I.C. Plus, EPRI) equipped with an anion separation column (Metrosep A Supp 5–100/4.0, Metrohm, EPRI). The efficiency of the membrane used was regularly checked with the NaCl rejection before starting each run. The samples were measured triplicated for each study in the membrane dead-end system. The concentrations of dyes in permeate and feed solutions were defined using UV–Vis spectroscopy (UV-2500 PC, Shimazu), at the wavelength range of 464 nm and 664 nm. The rejection ratio (R%) of the dyes was expressed as shown in Eq. 1.

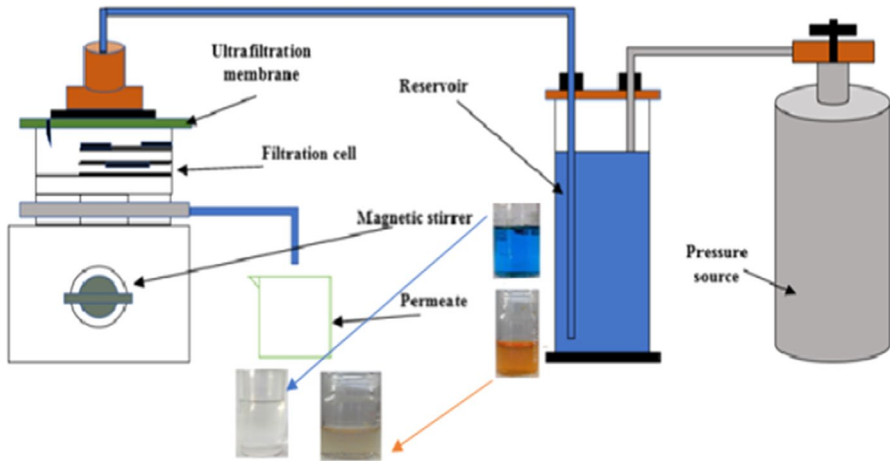**Fig. 1** Ultrafiltration setup has a filtration cell, ultrafiltration membrane, magnetic stirrer, pressure source, and reservoir

$$R\% = \left(1 - C_\mathrm{p}/C_\mathrm{f}\right) * 100 \tag{1}$$

whereas, the concentrations of dyes in permeate, and feed sides, are C_p and C_f, respectively.

Membrane regeneration

Membrane cleaning was performed with 0.01 N HCl and NaOH according to the feed dye solution and/or distilled water for 60 min for 7 cycles. The permeate samples from the membrane module were collected and analyzed after a certain time of operation. UV–Vis spectroscopy was used to analyze the dyes in permeate and feed solutions. A spectrophotometer was carried out after the sample solutions were acidified with HCl.

Characterization

The surface morphology and functional groups of the fabricated samples (ESPA and ESPA-WB nanocomposite membrane before and after dyes uptake) were characterized by scanning electron microscopy technique (SEM), JSM-6700F, JEOL, Tokyo, Japan, acting space of 11.1 to 12.2 mm, beam energy: 20–30 kV) [60], and Fourier transform infrared spectroscopy (FTIR) spectroscopy (Bruker VERTEX 70, Germany, with an ATR sampling accessory MIRacle, Pike Technology, Inc. ranged from 4000 to 500 cm^{-1} with resolution 4 cm^{-1} at room temperature), respectively. Fiber diameters were quantitatively measured using Image J software. The conductivity of the solutions was measured by using Wissenschaftlich-Technische-Werksta̎tten WTW and 315i = SET apparatus.

While the crystallinity and surface area characteristics of the ESPA and ESPA-WB membranes were obtained by the X-ray diffraction (XRD) patterns (Philips APD-3720 diffractometer, where the X-ray supply is Cu Kα radiation, that working at 40 mA and 40 kV with a 5°/min at 5–80 degrees (2θ) range) [61] and Surface Area Analyzer (Nova 2000 Quantachrome, samples degassed in a vacuum at 100 °C for 2 h to clean the samples surfaces and pores from the contaminants), respectively. Brunauer-Emmetand Teller model was used to determine the BET surface area while the Barrett–Joyner–Halenda (BJH) formula was used to calculate the pore volume and size.

Results and discussion

SEM analysis

Figure 2a, b demonstrate the surface SEM images of both the ESPA and ESPA-WB membranes. The SEM image of the ESPA membrane (Fig. 2a) was decided as a uniform structure having a small pore in the nano-scale. The SEM image of the
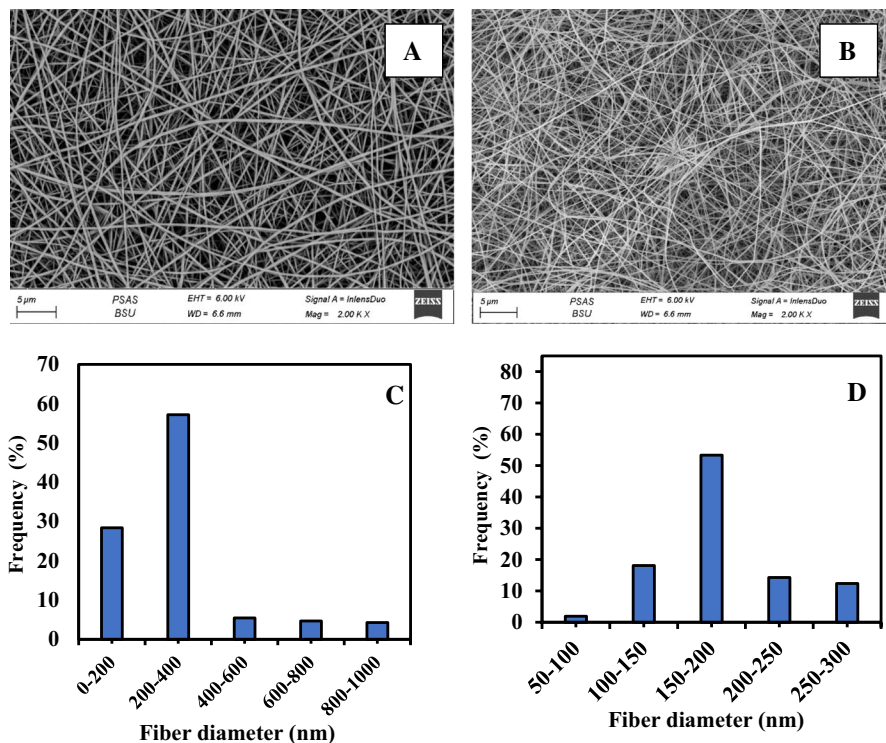

Fig. 2 SEM of **a** ESPA, **b** ESPA-WB, and the fiber diameter distribution histogram plots of **c** ESPA and **d** ESPA-WB

ESPA-WB (Fig. 2b) revealed that the presence of WB increased surface roughness [62]. As well, the degree of cross-linking and diameter of fibers was also improved due to the interaction between WB and PA components. Thus, this leads to an active layer being developed on the pristine membrane as seen from the increase in the rejection of the membrane for the two dyes [63]. Additionally, the fiber diameter distribution histogram plots that were derived from the SEM pictures using the Image J software [65] (Fig. 2c, d), showed a noticeable difference in the diameter of ESPA-WB fiber relative to that of ESPA. The fiber average diameter of ESPA was about 294.57 nm with standard deviation of 176 (Fig. 2a, c). Whereas, that of the ESPA-WB was 188.96 nm with standard deviation of 51 (Fig. 2b, d). The perceptible reduction in the average diameter of fibers and the improvement of its distribution with WB incorporation can be attributed to the increase in the conductivity of the electrospinning solution. This was supported by the conductivity measurements that were conducted for both solutions (WB-free and WB-bearing solutions of ESPA and ESPA-WB membranes, respectively). Such measurements revealed that the incorporation of WB increased the conductivity from 10.2 µS/cm for ESPA to 42.2 µS/cm in the case of ESPA-WB. This increase can be ascribed to the increase in the number of mobile ions in the solution owing to the enrichment of WB with several metal oxides such as MgO, FeO, CaO, etc.. [58]

X-ray diffraction

The X-ray diffraction analysis of the ESPA and ESPA-WB shows the patterns of a predominant amorphous material with some crystallinity (Fig. 3a). In this sense, the bands around 19.87° and 23.67° correspond to the reflection of (100) and (010, 110) of α-phase of nylon 6.6 crystals oriented in a triclinic cell. The α^1 phase corresponds to the distance between adjacent chains of nylon 6.6, interacting through hydrogen bonding, while the α^2 phase is attributed to the distance between lamellae of the polymer [66]. A couple of bands attributed to the α phase were more intense for the ESPA sample than for the ESPA-WB. In the case of ESPA-WB, weak diffraction peaks were observed in the diffraction patterns (Fig. 3a), which may come from the I_α polymorph of WB, which interconnected and increases the network of PA fibers during the electrospinning process of the membranes. The diffractograms of the ESPA-WB show peaks at 20.4°, 21.6°, 23.6°, and 27.7° with crystalline plans (200) and (002, 202), attributed to the crystalline phases of nylon 6.6 and WB, respectively; these signals have nearly the same intensity. We found also that the same peaks of PA fibers remain after the incorporation of the WB particles whose presence is confirmed for the new peaks observed. The intensity of the crystalline plan (002, 202) is lower than the intensity of the reflection (200) which indicates that the WB particles favor the formation of the α_2 phase in the ESPA-WB matrix [66]. This behavior has been previously reported by other authors in spherical nanoparticles dispersed in nylon 6.6; these authors concluded that this phenomenon is closely related to a secondary crystallization process, where crystal growth is held onto the crystalline phase with a higher energy level [67].
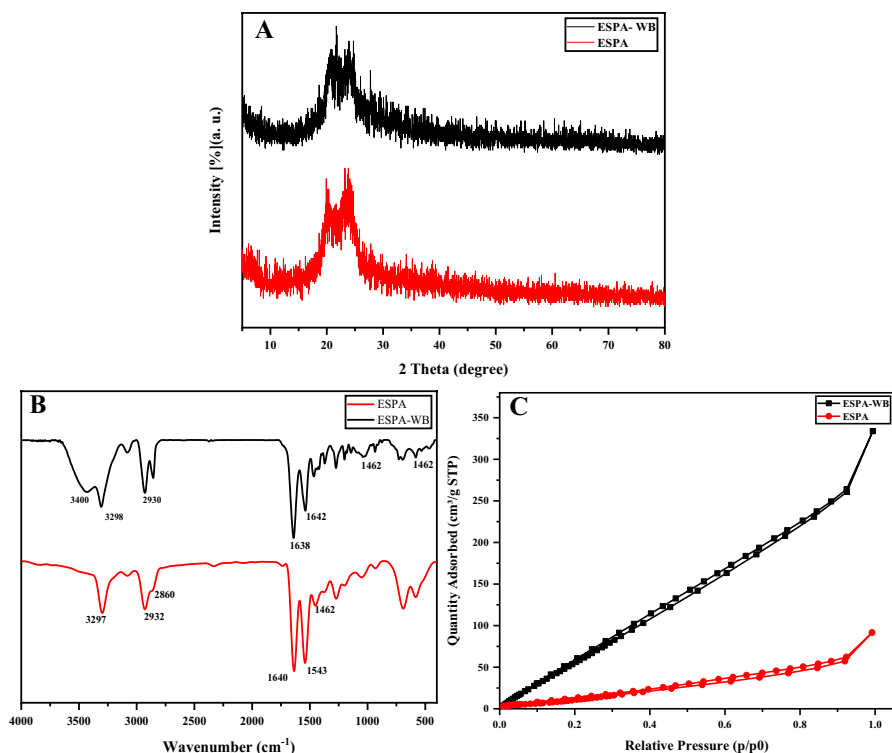
Fig. 3 **a** XRD of ESPA and ESPA-WB, **b** FTIR of ESPA and ESPA-WB, and **c** Nitrogen adsorption/desorption isotherms of ESPA and ESPA-WB membranes

FTIR spectroscopy

FTIR spectra of ESPA and ESPA-WB are presented in Fig. 3b. As shown in Fig. 3b, the band appearing at 1543 cm^{-1} is due to N–H deformation (Amide II). The appearance of Amide I and Amide II peaks indicates the formation of the ESPA matrix [68]. The absorption peak at 3297 cm^{-1} is due to the stretching vibration of N–H, the peaks at 2932 cm^{-1} and 2860 cm^{-1} are due to –CH$_2$– stretching, the peak at 1640 cm^{-1} is due to C=O stretching that generally overlapped with amide I, and the peak at 1462 cm^{-1} is due to the specific N–H bending peak of ESPA [68]. The broad bands noticed at 3400, 3298, and 2930 cm^{-1} with dissimilar strengths and positions may be for the O–H group of WB in ESPA-WB [69]. The stretching and bending vibrations of Si–O–Si in silicates appeared at 1038 cm^{-1} and 579 cm^{-1}, respectively. In addition, a strong band appeared at 1638 cm^{-1} was assigned to $-$OH deformation of H$_2$O molecules. However, the peak that appears at 1542 cm^{-1} is corresponding to the C=O absorption band of WB [64].

BET analysis

Table 1 presents the pore size, pore volume, and surface area determined by both BET analysis and N_2 adsorption/desorption isotherm [43]. It is noticeable that most of the pores obtained from the analysis lie between 2 and 3 nm, and this indicates that the distributions between the pore sizes are very narrow. It's found that the average pore diameter produced for ESPA and ESPA-WB membranes are 2.816 and 2.193 nm, respectively. Meanwhile, the average pore volume for the same two membranes obtained using the N_2 adsorption/desorption isotherm analysis as shown in Fig. 3c is 0.1418 and 0.652 cc/g, respectively. As shown in Fig. 3c, the N_2 adsorption–desorption isotherm of the ESPA and ESPA-WB membranes belongs to the type II isotherm of IUPAC. Such isotherms indicate that the pores of the material are macropores and mesopores. Its linear shape reflected the unrestricted single-layer adsorption, and the inflection point of the curve was not obvious, indicating that the coverage of the monolayer was superimposed with the initial amount of multilayer adsorption. The ESPA-WB membrane had a higher specific surface area ($350.5 \mathrm{~m^2~g^{-1}}$) than the ESPA. This indicates the good compatibility between the two determination methods [47]. Finally, it can be concluded from this analysis that the preparation of ESPA and ESPA-WB were investigated efficiently [48].

Membrane adsorption process

Effect of pH

The pH value is one of the most important factors affecting the adsorption process. To investigate the influence of pH on the MO and MB removal by ESPA and ESPA-WB, in such experiments, the pH range between 2.5 and 10.0 and the dye concentration of 125 mg/L were chosen. In Fig. 4, the highest removal efficiencies of ESPA at pH 9.5 for MO and MB, respectively, are approximately 34.8% and 70.45% whereas, the maximum efficiencies of ESPA-WPS are 48.32% and 73.2%, respectively [49]. We also noted that the removal efficacy of MB dye (as a positively charged molecule), increased when the pH values increased from 2.5 to 9.5 due to the reduction in the attraction force. Whereas, for MO dye the lowest removal efficacy is correlated to a pH of 9.5 that no repulsive force or exclusion is important.

This can be explained by the fact that rising the pH of the dye solution accelerates the binding of the positive cations of the MB dye with the negative charged functional groups on the adsorbent membrane surface. Also, the pH may affect the rejection of the membranes due to charge exchange and changing the membrane surface

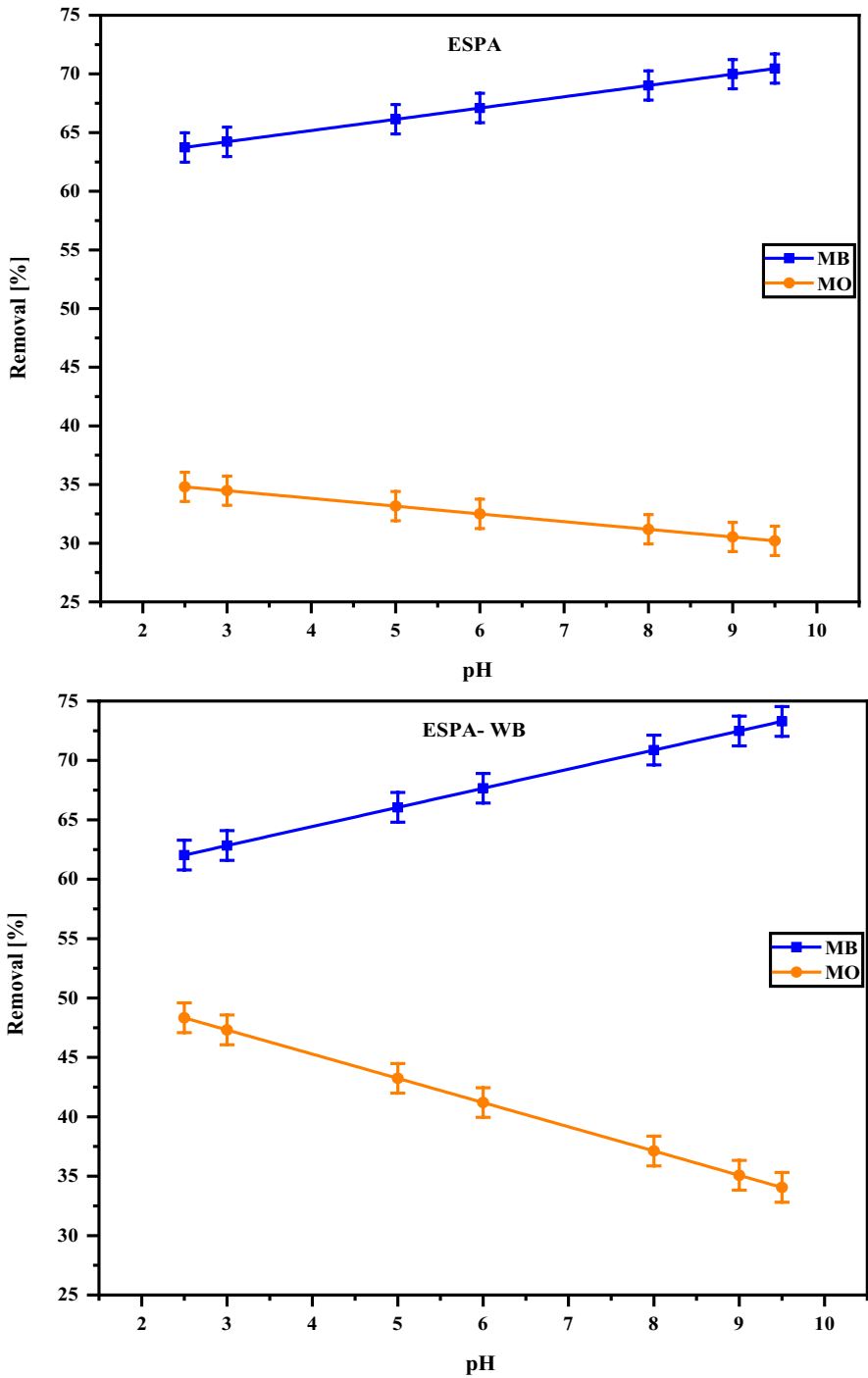| Table 1 Surface textures of ESPA and ESPA-WB	Membrane	SA (m²/g)	Pore volume (cc/g)	Pore diameter (nm)
	ESPA	75.42	0.1418	2.816
	ESPA-WB	350.5	0.652	2.193

Fig. 4 Influence of pH on the MO and MB removal by ESPA and ESPA-WB

composition due to the dissociation of its functional groups. This is what happened in this study, where the increase in the pH values of MO and MB dyes' solutions, led to shrinking the pore size of ESPA and ESPA-WB membranes thus increasing the degree of ESPA and ESPA-WB membranes rejection.

Several parameters such as the adsorption capacity of the adsorbent, surface charges, and active sites might be attributed to the adsorption behavior of the adsorbent at various pHs. The surface of ESPA and ESPA-WB contains a large number of active sites. The dye uptake can be related to the active sites and also to the chemistry of the dye in the solution. Theoretically, at pH < isoelectric point, the surface gets positively charged, which enhances the adsorption of the negatively charged dye anions through electrostatic forces of attraction. At pH > isoelectric point, the surface of ESPA and ESPA-WB gets negatively charged, which favors the adsorption of cationic dyes [70].

It was found that the pH of the ESPA-WB membrane at the isoelectric point (IP) is 6.2, after that, the membrane become has negative charges, due to the adsorption of more hydroxyl ions on its surface, because, after the IP, the repulsive electromotive force between the ESPA-WB membrane surface and the negatively charged particles increases. Moreover, at a pH lower than IP, the ESPA-WB membrane surface has a more positive charge than the ESPA membrane, thus the removal of positively charged contaminants such as methylene blue dye is more effective [51].

Effect of dye initial concentration

The initial dye concentration is a significant feature of the adsorption performance of adsorbent material. As shown in Fig. 5, increasing dyes (MB and MO) concentration, led to growing the uptake efficiency, due to growing the space prevention and impact size exclusion. Dye removal experiments were performed at different concentrations of dyes (20–120 mg/L), to reach a steady state, by adjusting the pressure rate and at the same initial water flow [71].

When the dye concentrations were increased with constant pH, the negative charge on the surface of the ESPA and ESPA-WB membranes, led to an increase in the repulsive force between the membranes surface and the dye molecules. Figure 5 viewings the percentage of uptaking MO dye onto ESPA and ESPA-WB membranes at different initial dye concentrations of 20–120 mg/L. It was found that the uptake efficacy of MO dye decreases when the concentration of the positively charged dye increased by passing more molecules through the ESPA and ESPA-WB membranes at constant pressure and pH [55]. At high MO dye concentration, the adsorption process and the uptake efficiency are reduced.

It was found that the ESPA-WB membrane succeeds to remove 74% of MO dye concentration at 20 mg/L, which means, a very fast uptake. With increasing the initial MO dye concentration, the adsorption processes of MO dye solution onto the ESPA-WB membrane surface decrease, and thus the efficiency of its uptake decreases. Note that at the same time of adsorption onto the ESPA-WB membrane surface, the concentration of MO dye solution increases, and its uptake percentage decreases [56]. This can be attributed to the fact that the polyamide (PA) matrix has
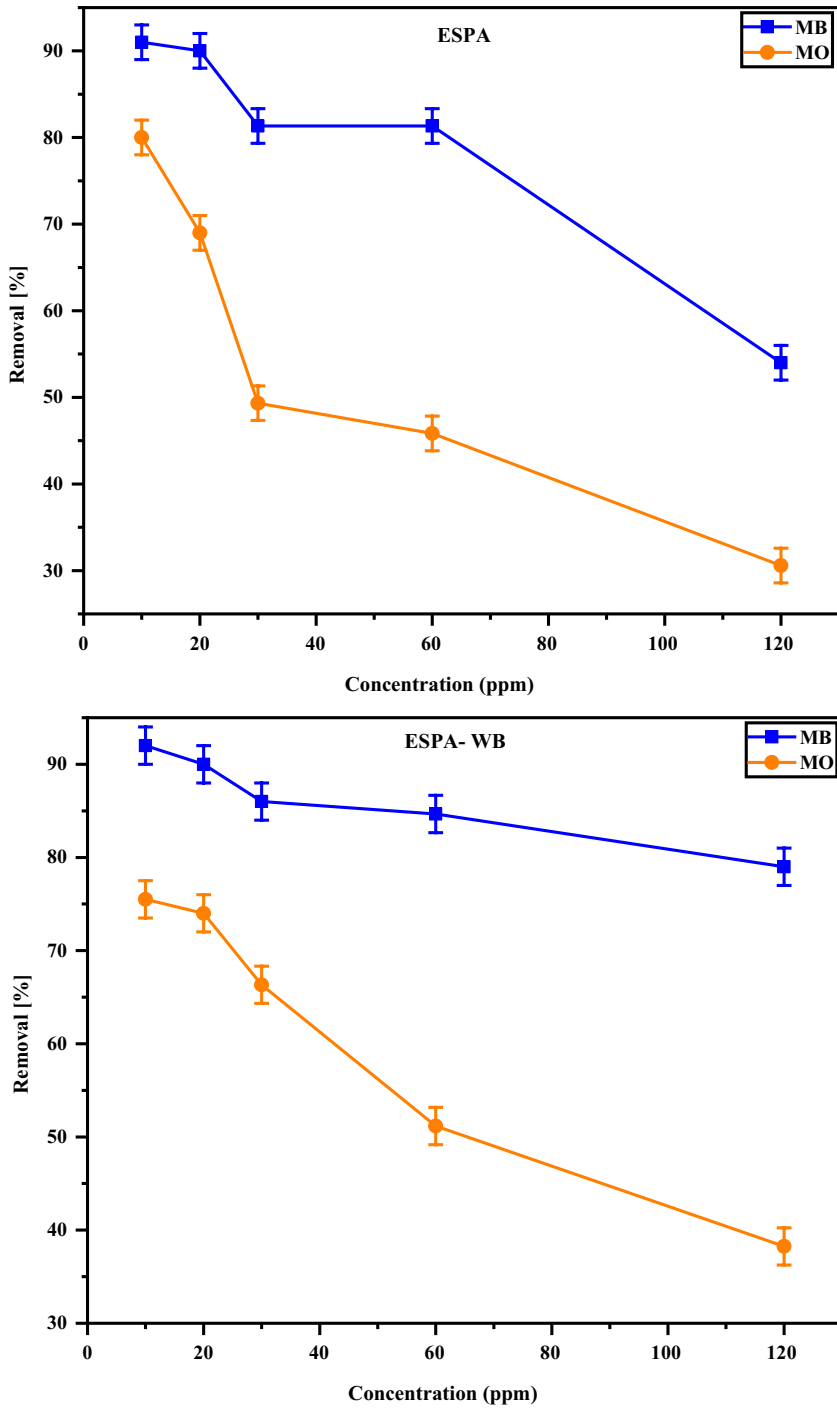
Fig. 5 Effect of initial dye concentration change on ESPA-WB membranes rejection of MB and MO dyes

a maximum saturation limit, after which the polymer cannot completely remove the dye.

Effect of electrolyte completions

The ESPA and ESPA-WB membranes were employed for the filtration of mixed solutions of crystal violet dye/inorganic salt. The results of equilibrium flux flow and dye uptake degree versus the dye/salt mixtures at different dye concentrations onto ESPA and ESPA-WB membranes are shown in Fig. 6a, b. Thus, it is found that the initial rejection rate of the two membranes is slightly different and the effect of flood strain on the dying of both ESPA and ESPA-WB membranes is analogous [72]. From the results, it is clear that the MB dye can be completely removed from the dye/salt mixture using the two membranes, and that there are significant differences in the dye removal rate and its concentration change between the two membranes. The membrane was further employed for the filtration of another dye solution: MO. The ESPA-WB membrane displayed high rejection for MB (95, 91.2, and 83.8%) with salts NaOH, NaCl, and $CaCl_2$, respectively. In the case of MO, the rejection rate is 83.5, 54, and 61.6% for NaOH, NaCl, and $CaCl_2$, respectively. The reason was that the pore size of ESPA-WB is much larger than the sizes of the hydrated salt ions (0.66–1.0 nm) [72]. Therefore, the ESPA-WB membrane can be used for the purification of dye products containing salts. As compared with other NF membranes [73–75], the obtained ESPA-WB membranes showed a higher rejection rate for the same dyes. The staggered pores (2.1 nm) of the ESPA-WB membrane render a high rejection for dyes together with a fast transport of salt and solvents than in the case of the ESPA membrane (Fig. 6a, b).

Effect of pressure

Figure 7 reveals that when the pressure increases from 0.5 to 24 bar, the removal efficiency for both acid and disperse dyes is increased [61]. In contradiction, an extra pressure increase led to a slight reduction in the uptake efficacy. In the case of positively charged methylene blue dye, increasing the pressure had a negative effect on the uptake efficacy because more dyes were passed through the membrane as seen in Fig. 7 [62].

Repeatability cycles and properties of membranes

Membrane repeat experiments were performed to study the repeatability of the prepared ESPA and ESPA-WB membranes. Figure 8 shows the membrane separation performance in terms of salt rejection. The results indicate that the repeatability of the prepared membranes is satisfactory.

The ESPA-WB membrane achieve an average trial-to-trial rejection performance of 82.5 and 65% for MB and MO dyes, respectively, at 120 mg/L dye aqueous solution and 24 bar operating pressure, in addition, the ESPA-WB membrane gave an average trial-to-trial performance of 7 cycles under the same conditions. We found that after 7 cycles, the rejection remained above 66% and 49% for
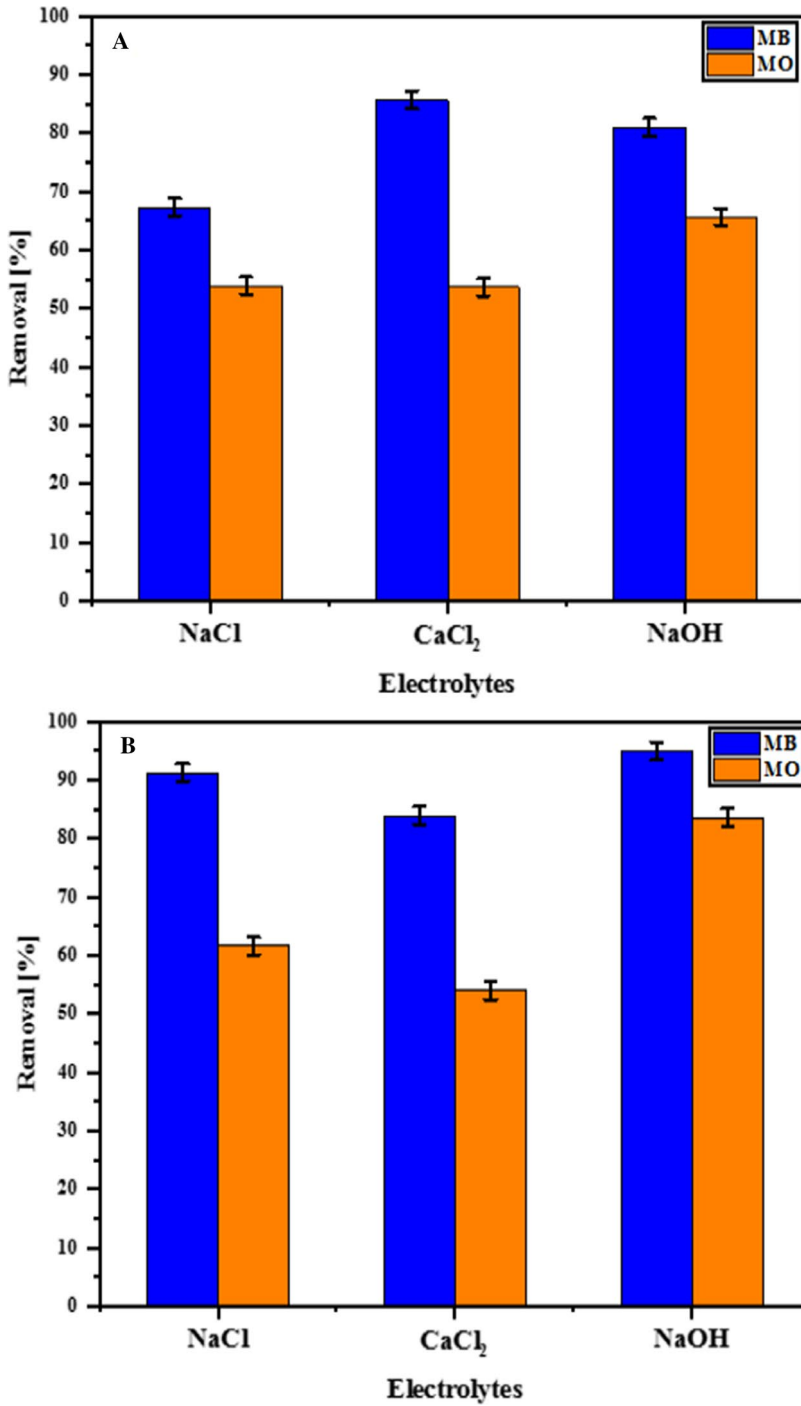
Fig. 6 Effect of electrolyte change on **a** ESPA and **b** ESPA-WB membranes rejection of MB and MO dyes
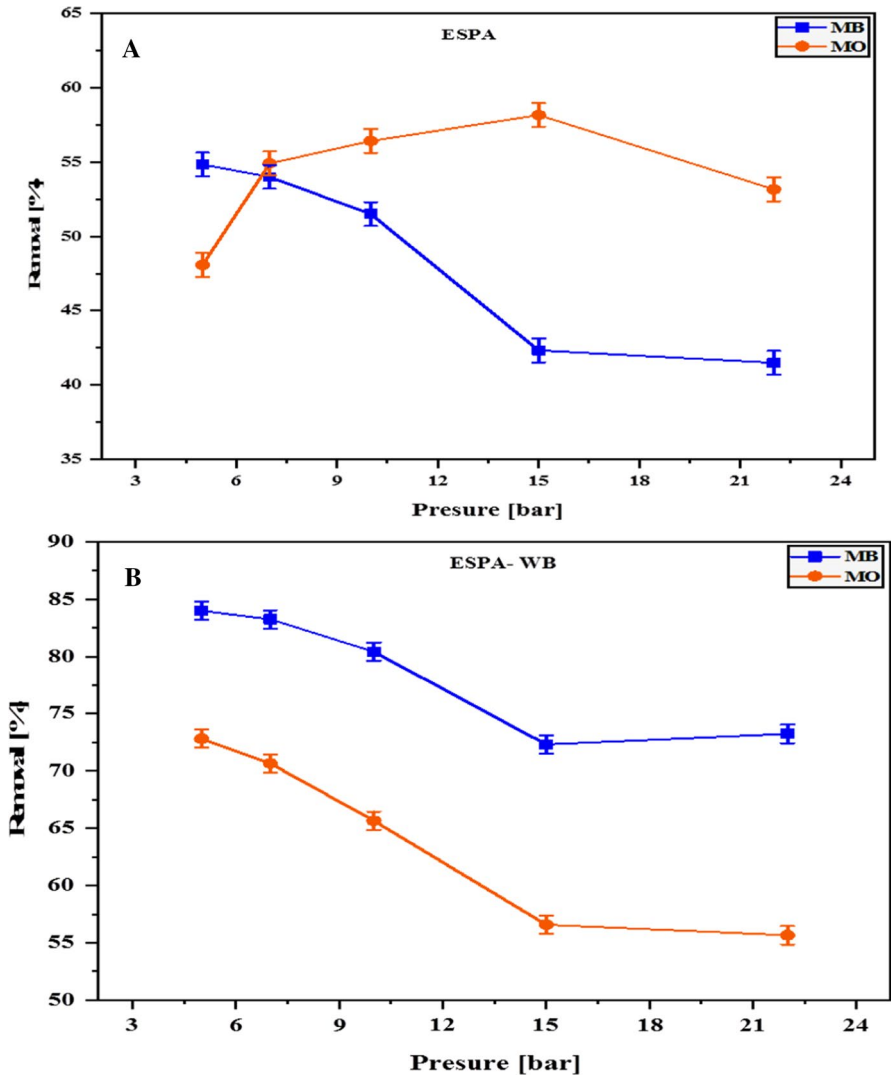
Fig. 7 Effect of pressure change on **a** ESPA and **b** ESPA-WB membranes rejection of MB and MO dyes

MB and MO dye, respectively [76]. It's noted that the performance of fiber membrane adsorption is decreased after five cycles of regeneration. This is because the texture of the fiber membrane itself was relatively soft, and repeated adsorption cycles cause blockage of the fiber pores of the membrane and damage the fiber structure to a certain extent. In the control experiments, the adsorption of membrane for dyes demonstrated that the rejection was mainly ascribed to the pore-sieving mechanism and chemisorptions mechanism according to dye type [77]. These results indicate that the ESPA-WB membrane had regeneration performance in the adsorption of MB and MO.
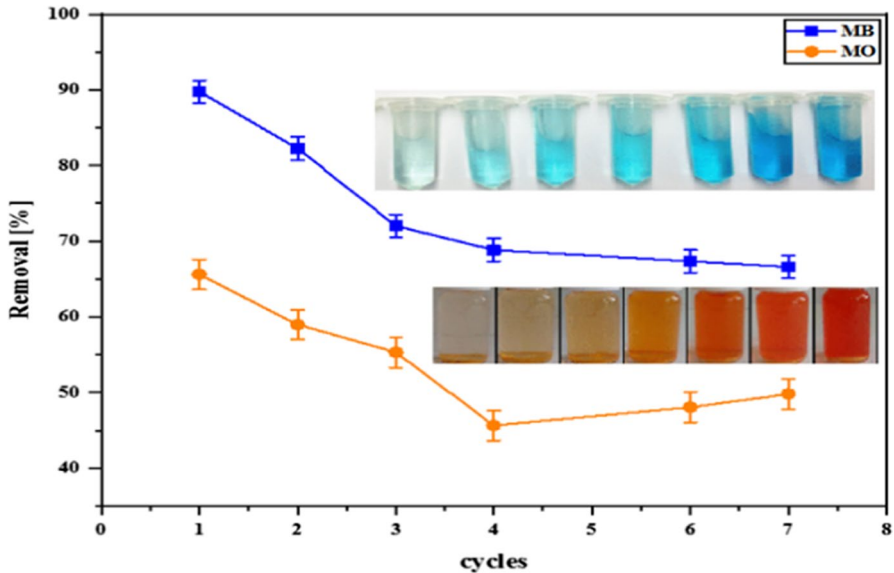
Fig. 8 Effect of the regeneration cycles on ESPA-WB membrane rejection of MB and MO dyes

Also, the images inserted into Fig. 8 show the noticeable color change with the increase in the number of reuse cycles of the membranes. It can be noticed from Fig. 8 that the color intensity of MB increases from left to right with the increase in the number of cycles, and similarly in the case of MO.

Mechanism of adsorption process simulation

We can conclude that the mechanism and efficiency of adsorption of MO and MB dyes onto the surface of the prepared membrane depend mainly on the pH of the dye solution [65]. Under acidic conditions, the surface of the ESPA-WB membrane possesses a positive charge and exists in its protonated form.

Figure 9a–c shows the combining of SEM and FTIR analysis after the adsorption of MB and MO dyes onto the ESPA-WB membrane surface to determine the mechanism of adsorption

Based on this analysis, it can be seen that the dominant factor in the adsorption process mainly is a physical effect, i.e., electrostatic attraction via the insertion of MB and MO molecules inside the hollow structure of the ESPA-WB membrane [70, 71].

The high removal efficiency of MB can be discussed according to the presence of; (1) Strong hydrogen bonds, i.e., strong chemical interaction, and (2) The existence of electrostatic attraction between the positively charged MB dye and the anionic ESPA-WB membrane surface. The decrease in the adsorption performance of MO dye is due to the following reasons; (1) There is no chance of hydrogen bond formation between the ESPA-WB membrane and the MO dye in the basic medium. (2) The low concentration of hydroxyl ions reduces the negative charge density on
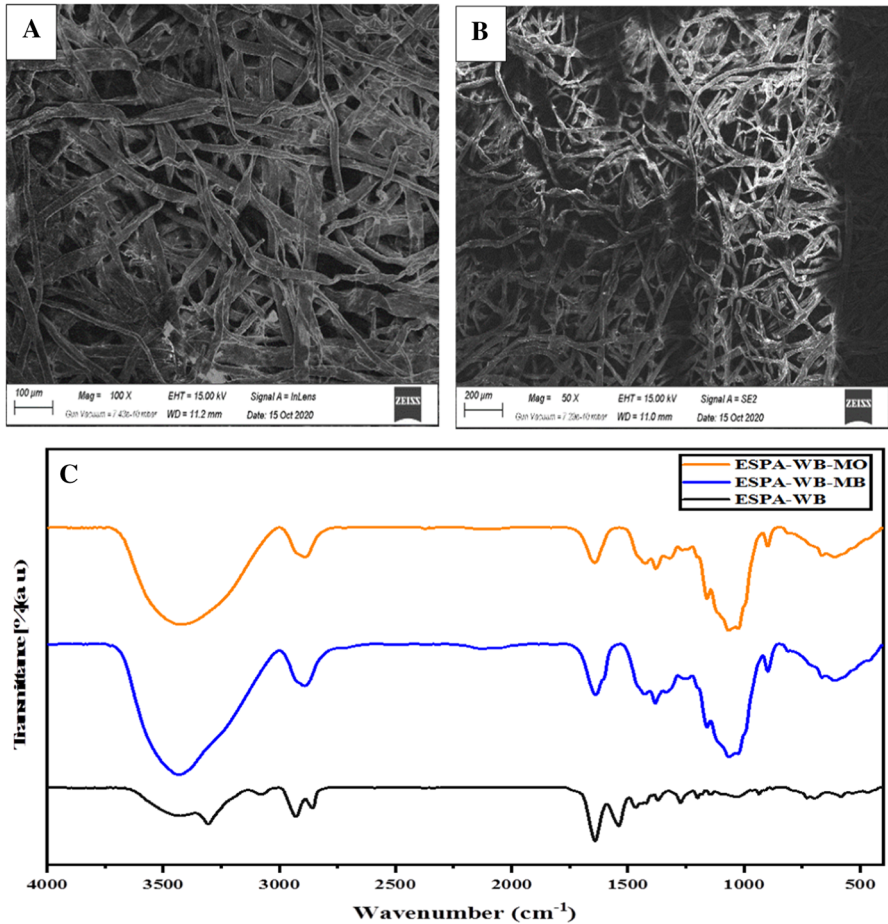
Fig. 9 SEM analysis of ESPA-WB membrane after **a** MB and **b** MO dyes adsorption and FTIR of ESPA-WB membrane before and after dyes adsorption

the ESPA-WB membrane surface which causes the formation of protons on the ESPA-WB membrane (due to the presence of NH$^+$ centers); thus, the adsorption process decreases [69].

Conclusion

In this work, the development of polymeric membranes for adsorbing toxic dyes is a challenge, so, we aim to prepare two superior and recyclable novel adsorbent materials (ESPA and ESPA-WB) for adsorbing toxic dyes. By comparing the ESPA membrane with the ESPA-WB membrane, it was found that the latter is characterized by its high recyclability, and its efficiency in removing methylene blue (MB) and

methyl orange (MO) dyes because it is a mixture of ESPA membrane and Weathered basalt (WB). Hence, its efficiency was improved for the following reasons: (1) increasing the sum of the active binding sites, and (2) improving the reaction due to the formation of new functional groups that favor the adsorption of dye molecules. Furthermore, to achieve the applicability of the ESPA-WB composite membrane towards MB and MO dye adsorption, filtration adsorption experiments were performed with different doses, pH, and dye concentrations. Also, after blending, the surface of the fibers became smoother and their diameter increased, while the morphology of the nanofibers did not significantly change. The best results for removal efficiency were reported at pH 9 and 3 for MB and MO dye, with the uptake percentages of more than 99% and 70%, respectively. Therefore, the prepared ESPA-WB electrospun nanocomposite membrane could be a good candidate for the treatment of dye-bearing wastewater.

References

1. Varjani S et al (2020) Microbial degradation of dyes: an overview. Biores Technol 314:123728
2. Chiong T et al (2016) Enzymatic treatment of methyl orange dye in synthetic wastewater by plant-based peroxidase enzymes. J Environ Chem Eng 4(2):2500–2509
3. Bai L et al (2019) Kinetics and mechanism of photocatalytic degradation of methyl orange in water by mesoporous Nd-TiO$_2$-SBA-15 nanocatalyst. Environ Pollut 248:516–525
4. Seenuvasan M et al (2013) Fabrication, characterization and application of pectin degrading Fe$_3$O$_4$–SiO$_2$ nanobiocatalyst. Mater Sci Eng, C 33(4):2273–2279
5. Wang L et al (2019) Enhanced photocatalytic degradation of methyl orange by porous graphene/ZnO nanocomposite. Environ Pollut 249:801–811
6. Chen P et al (2020) Synthesis of unique-morphological hollow microspheres of MoS2@montmorillonite nanosheets for the enhancement of photocatalytic activity and cycle stability. J Mater Sci Technol 41:88–97
7. Khaki MRD, Shafeeyan MS (2020) Sol–gel synthesized ZnO/Mn–TiO$_2$ core–shell nanocomposite and its elevated activity for methyl orange degradation. J Nanophoton 14(03):111. https://doi.org/10.1117/1.JNP.14.036015
8. Ye Y et al (2017) Homogeneous photosensitized degradation of pharmaceuticals by using red light LED as light source and methylene blue as photosensitizer. Chem Eng J 316:872–881
9. Nagar N, Devra V (2019) A kinetic study on the degradation and biodegradability of silver nanoparticles catalyzed Methyl Orange and textile effluents. Heliyon 5(3):e01356–e01356

10. Ahmed HA, Mubarak MF (2021) Adsorption of cationic dye using a newly synthesized CaNiFe$_2$O$_4$/chitosan magnetic nanocomposite: kinetic and isotherm studies. J Polym Environ 29(6):1835–1851

11. Javaid R, Qazi UY (2019) Catalytic oxidation process for the degradation of synthetic dyes: an overview. Int J Environ Res Public Health 16(11):2066

12. Dellamatrice PM et al (2017) Degradation of textile dyes by cyanobacteria. Br J Microbiol 48(1):25–31

13. Solyman S, Ahmed HA (2021) Treatment of industrial dye effluent by photo-catalytic process using modified Egyptian Bentonite. Egypt J Chem. https://doi.org/10.21608/ejchem.2021.92237.4376

14. Cuerda-Correa EM, Alexandre-Franco MF, Fernández-González C (2019) Advanced oxidation processes for the removal of antibiotics from water. An Overv Water 12(1):102

15. Liu M et al (2017) High efficient removal of dyes from aqueous solution through nanofiltration using diethanolamine-modified polyamide thin-film composite membrane. Sep Purif Technol 173:135–143

16. Lin J et al (2015) Fractionation of direct dyes and salts in aqueous solution using loose nanofiltration membranes. J Membr Sci 477:183–193

17. Ma Z, Kotaki M, Ramakrishna S (2005) Electrospun cellulose nanofiber as affinity membrane. J Membr Sci 265(1–2):115–123

18. Kim T-H, Park C, Kim S (2005) Water recycling from desalination and purification process of reactive dye manufacturing industry by combined membrane filtration. J Clean Prod 13(8):779–786

19. Kebria MRS, Jahanshahi M, Rahimpour A (2015) SiO2 modified polyethyleneimine-based nanofiltration membranes for dye removal from aqueous and organic solutions. Desalination 367:255–264

20. Song J, Kim M, Lee H (2020) Recent Advances on nanofiber fabrications: unconventional state-of-the-art spinning techniques. Polymers 12(6):1386

21. Huang Y et al (2019) Scalable manufacturing and applications of nanofibers. Mater Today 28:98–113

22. Xu Y et al (2019) Functionalized polyethersulfone nanofibrous membranes with ultra-high adsorption capacity for organic dyes by one-step electrospinning. J Colloid Interface Sci 533:526–538

23. Kaur S et al (2014) the characterization of electrospun nanofibrous liquid filtration membranes. J Mater Sci 49(18):6143–6159

24. Hasanzadeh M, Hadavi Moghadam B (2013) Electrospun nanofibrous membranes as potential adsorbents for textile dye removal:-a review. J Chem Health Risks **3**(2):15–26

25. Heikkilä P et al (2008) Electrospinning of polyamides with different chain compositions for filtration application. Polym Eng Sci 48(6):1168–1176

26. Dharmaraj N et al (2006) Spectral studies of SnO2 nanofibres prepared by electrospinning method. Spectrochim Acta Part A Mol Biomol Spectrosc 64(1):136–140

27. Wang C et al (2007) Preparation of one-dimensional TiO$_2$ nanoparticles within polymer fiber matrices by electrospinning. Mater Lett 61(29):5125–5128

28. Carrizales C et al (2008) Thermal and mechanical properties of electrospun PMMA, PVC, Nylon 6, and Nylon 6,6. Polym Adv Technol 19(2):124–130

29. Macossay J et al (2007) Effect of needle diameter on nanofiber diameter and thermal properties of electrospun poly(methyl methacrylate). Polym Adv Technol 18(3):180–183

30. Youn D-Y et al (2011) Facile synthesis of highly conductive RuO$_2$-Mn$_3$O$_4$ composite nanofibers via electrospinning and their electrochemical properties. J Electrochem Soc 158(8):A970

31. Zhou H, Touny AH, Bhaduri SB (2011) Fabrication of novel PLA/CDHA bionanocomposite fibers for tissue engineering applications via electrospinning. J Mater Sci Mater Med 22(5):1183–1193

32. Cui Q et al (2008) Direct fabrication of cerium oxide hollow nanofibers by electrospinning. J Rare Earths 26(5):664–669

33. Wang G et al (2017) Electrospun nanofiber: Emerging reinforcing filler in polymer matrix composite materials. Prog Polym Sci 75:73–107

34. Opálková Šišková A et al (2021) Electrospun poly(ethylene terephthalate)/silk fibroin composite for filtration application. Polymers 13(15):2499

35. Ahne J et al (2018) Electrospun cellulose acetate nanofibers for airborne nanoparticle filtration. Text Res J 89(15):3137–3149

36. Liu Y et al (2021) Electrospun antibacterial and antiviral poly(ε-caprolactone)/zein/Ag bead-on-string membranes and its application in air filtration. Mater Today Adv 12:100173

37. Zulfi A et al (2018) Air filtration media from electrospun waste high-impact polystyrene fiber membrane. Mater Res Express 5(3):035049

38. Xu X et al (2020) Biodegradable engineered fiber scaffolds fabricated by electrospinning for periodontal tissue regeneration. J Biomater Appl 36(1):55–75

39. Liu H et al (2019) Transparent antibacterial nanofiber air filters with highly efficient moisture resistance for sustainable particulate matter capture. iScience 19:214–223

40. Wang Z, Zhao C, Pan Z (2015) Porous bead-on-string poly(lactic acid) fibrous membranes for air filtration. J Colloid Interface Sci 441:121–129

41. Kim H-J et al (2021) Eco-friendly poly(vinyl alcohol) nanofiber-based air filter for effectively capturing particulate matter. Appl Sci 11(9):3831

42. Ding Y et al (2016) Electrospun polyimide nanofibers and their applications. Prog Polym Sci 61:67–103

43. Bhardwaj N, Kundu SC (2010) Electrospinning: a fascinating fiber fabrication technique. Biotechnol Adv 28(3):325–347

44. Li D, Xia Y (2004) Electrospinning of nanofibers: reinventing the wheel? Adv Mater 16(14):1151–1170

45. Deitzel JM et al (2001) The effect of processing variables on the morphology of electrospun nanofibers and textiles. Polymer 42(1):261–272

46. Laudenslager MJ, Sigmund WM (2012) Electrospinning. In: Bhushan B (ed) Encyclopedia of nanotechnology. Springer, Berlin, pp 769–775

47. Ramakrishna S (2005) An introduction to electrospinning and nanofibers. World Scientific, Singapore

48. Novotna K et al (2019) Microplastics in drinking water treatment—current knowledge and research needs. Sci Total Environ 667:730–740

49. Stanescu MD (2021) State of the art of post-consumer textile waste upcycling to reach the zero waste milestone. Environ Sci Pollut Res 28(12):14253–14270

50. Ucar M, Wang Y (2011) Utilization of recycled post consumer carpet waste fibers as reinforcement in lightweight cementitious composites. Int J Cloth Sci Technol 23(4):242–248

51. Chen H-L, Burns LD (2006) Environmental analysis of textile products. Cloth Text Res J 24(3):248–261

52. Herzog B, Kohan MI, Mestemacher SA, Pagilagan RU, Redmond K (2013) Polyamides. In: Ullmann's encyclopedia of industrial chemistry. Wiley-VCH Verlag GmbH & Co. KGaA. https://doi.org/10.1002/14356007.a21_179.pub3

53. Žagar E et al (2020) Quantitative determination of PA6 and/or PA66 content in polyamide-containing wastes. ACS Sustain Chem Eng 8(31):11818–11826

54. Opálková Šišková A, Frajová J, Nosko M (2020) Recycling of poly(ethylene terephthalate) by electrospinning to enhanced the filtration efficiency. Mater Lett 278:128426. https://doi.org/10.1016/j.matlet.2020.128426

55. Isık T, Demir MM (2018) Tailored electrospun fibers from waste polystyrene for high oil adsorption. Sustain Mater Technol 18:e00084

56. Jiang Q et al (2012) Preparation of carbon nanotube/polyaniline nanofiber by electrospinning. Proc Eng 27:72–76

57. Saleh M et al (2021) Fabrication of basalt embedded composite fiber membrane using electrospinning method and response surface methodology. J Appl Polym Sci 138(25):50599

58. Abdel-Latief MA et al (2021) A new insight upon the use of weathered basalt as alternative raw material in Portland clinker production. Ain Shams Eng J 12(1):885–896

59. Metwally BS et al (2018) Fabrication, characterization, and dye adsorption capability of recycled modified polyamide nanofibers. Egypt J Chem 61(5):867–882

60. Ahmed HA et al (2022) Facile synthesis and characterization of magnetic biopolymer nanocomposite and its application for preparing novel bioasphalt coating binder. Egypt J Chem. https://doi.org/10.21608/ejchem.2022.100891.4688

61. Mubarak MF, Zayed AM, Ahmed HA (2022) Activated Carbon/Carborundum@Microcrystalline Cellulose core shell nano-composite: synthesis, characterization and application for heavy metals adsorption from aqueous solutions. Ind Crops Prod 182:114896

62. Pipich V et al (2019) Morphology and porous structure of standalone aromatic polyamide films as used in RO membranes—an exploration with SANS, PALS, and SEM. J Membr Sci 573:167–176

63. Jadoon A et al (2021) Probing the role of hydrolytically stable, 3-aminopropyl triethoxysilane crosslinked chitosan/graphene oxide membrane towards Congo red dye adsorption. Curr Appl Phys 40:110–118

64. Abu Sharib ASAA et al (2021) Utilizing modified weathered basalt as a novel approach in the preparation of Fe_3O_4 nanoparticles: Experimental and theoretical studies for crystal violet adsorption. J Environ Chem Eng 9(6):106220

65. Salvado R, Silvy J, Dréan J-Y (2006) Relationship between Fibrous Structure and Spunbond Process. Text Res J 76(11):805–812

66. Lewis AL et al (2021) Effects of mineralogy, chemistry and physical properties of basalts on carbon capture potential and plant-nutrient element release via enhanced weathering. Appl Geochem 132:105023

67. Campoy I, Gómez MA, Marco C (2000) Small angle X-ray diffraction study of blends of nylon 6 and a liquid crystal copolyester. Polymer 41(6):2295–2299

68. Fan C et al (2021) Microplastic constituent identification from admixtures by Fourier-transform infrared (FTIR) spectroscopy: The use of polyethylene terephthalate (PET), polyethylene (PE), polypropylene (PP), polyvinyl chloride (PVC) and nylon (NY) as the model constituents. Environ Technol Innov 23:101798

69. Ghebleh Goydaragh M et al (2021) Predicting weathering indices in soils using FTIR spectra and random forest models. CATENA 204:105437

70. Haflich HM et al (2021) Effect of halides on polyamide-based membrane flux and monomer degradation during chloramination. J Membr Sci 639:119717

71. Krishnan J et al (2017) Effect of pH, inoculum dose and initial dye concentration on the removal of azo dye mixture under aerobic conditions. Int Biodeter Biodegrad 119:16–27

72. Hebbar RS et al (2018) Fabrication of polyetherimide nanocomposite membrane with amine functionalised halloysite nanotubes for effective removal of cationic dye effluents. J Taiwan Inst Chem Eng 93:42–53

73. Dutta M, Bhattacharjee S, De S (2020) Separation of reactive dyes from textile effluent by hydrolyzed polyacrylonitrile hollow fiber ultrafiltration quantifying the transport of multicomponent species through charged membrane pores. Sep Purif Technol 234:116063

74. Yang S-G et al (2020) Fluorescence microscopy tracking of dyes, nanoparticles and quantum dots during growth of polymer spherulites. Polymer 191:122246

75. Singh R, Sinha MK, Purkait MK (2020) Stimuli responsive mixed matrix polysulfone ultrafiltration membrane for humic acid and photocatalytic dye removal applications. Sep Purif Technol 250:117247

76. He L, Lei W, Liu D (2021) One-step facile fabrication of mechanical strong porous boron nitride nanosheets–polymer electrospun nanofibrous membranes for repeatable emulsified oil/water separation. Sep Purif Technol 264:118446

77. Li Y et al (2021) Flexible and free-standing pristine polypyrrole membranes with a nanotube structure for repeatable Cr(VI) ion removal. Sep Purif Technol 258:117981

Publisher's Note Springer Nature remains neutral with regard to jurisdictional claims in published maps and institutional affiliations.